IEEE Access
Multidisciplinary ⋮ Rapid Review ⋮ Open Access Journal

Received January 7, 2021, accepted January 25, 2021, date of publication January 28, 2021, date of current version February 9, 2021.

Digital Object Identifier 10.1109/ACCESS.2021.3055248

An Adaptive Off-Time Controlled DCM Flyback PFC Converter With Unity Power Factor and High Efficiency

HUAN LUO, (Member, IEEE), TIANLEI ZANG, (Member, IEEE), SHI CHEN, (Member, IEEE), AND BUXIANG ZHOU, (Member, IEEE)

College of Electrical Engineering, Sichuan University, Chengdu 610064, China

Corresponding author: Shi Chen (chenshi629@163.com)

This work was supported in part by the National Natural Science Foundation of China under Grant 51907097, and in part by the Science and Technology Planning Project of Sichuan Province of China under Grant 2020JDRC0049.

ABSTRACT Constant duty cycle controlled discontinuous conduction mode (DCM) flyback power factor correction (PFC) converter has the advantage of high power factor (PF) and the disadvantage of low efficiency. While, constant on-time (COT) controlled critical conduction mode (CRM) flyback PFC converter has the exact opposite features, besides its switching frequency varies in a line cycle, and the variation range is very large, which complicates the electromagnetic interference (EMI) design. In order to obtain both benefits of these two control methods, an adaptive off-time (AOT) control technique for DCM flyback PFC converter is proposed in this paper. By utilizing the output voltage and the amplitude of line voltage to adjust the off-time of the main switch, the magnetizing current of transformer exactly operates in CRM when the rectified input voltage gets the peak. Thus, the root-mean-square (RMS) current of the main switch and the diode, as well as the conduction loss can be effectively reduced, and high efficiency can be obtained. The proposed control technique also can achieve theoretical unity PF over universal input voltage range of 90∼264VAC. Moreover, its variation range of switching frequency is greatly reduced compared to that of COT control. A 60W prototype has been fabricated and tested in the laboratory and experimental results are presented to verify the effectiveness of the proposed method.

INDEX TERMS Adaptive control, flyback converter, power factor.

I. INTRODUCTION

Power factor correction (PFC) converters have been widely used in AC to DC power conversions to achieve high power factor (PF) and low total harmonic distortion (THD) of input current [1]–[6]. Flyback converter is one of the most popular topologies for the applications of PFC converter [7]–[14], because it exhibits lots of advantages, such as input and output isolation capability, simple structure, and low cost. Flyback PFC converters are commonly designed to operating at discontinuous conduction mode (DCM) and critical conduction mode (CRM) for the benefits of no reverse recovery of the freewheeling diode and simple control circuits.

Constant duty cycle control is usually utilized for DCM flyback PFC converter, which can achieve sinusoidal input current and unity PF. Besides, it operates in constant switching frequency, which is beneficial for the designing of input filter. However, the transfer of the energy does not cover the whole switch period, so that the peak current, as well as the root-mean-square (RMS) current flowing through the main switch at primary side and the diode at the secondary side are high, resulting in high conduction loss and low system efficiency. An optimum utilization control of switch cycles control strategy for DCM flyback PFC converter is proposed in [15]. By changing the duty cycle according to the rectified input voltage and output voltage, more energy can be transferred to the load within each switch period than that of constant duty cycle control, so the peak current and the RMS current are significantly reduced, however, the input current suffers from serious distortion, and the PF is low.

Compared to constant duty cycle controlled DCM flyback PFC converter, constant on-time (COT) controlled CRM

The associate editor coordinating the review of this manuscript and approving it for publication was Meng Huang.

flyback PFC converter can significantly reduce the peak current and RMS current, thereby achieving lower conduction loss and higher efficiency. However, COT controlled CRM flyback PFC converter cannot achieve unity PF, and the input current THD increases with the increase of input voltage. For LED applications, it is better to make THD less than 10% over universal input voltage range [16], while COT controlled CRM flyback PFC converter can hardly meet this requirement. Besides, the switching frequency of COT controlled CRM flyback PFC converter varies over each half-line cycle, and the variation range is very large, especially at high input voltage. The huge variation range of switching frequency will bring great difficulty in designing input filter, as the conducted electromagnetic interference (EMI) distributes in a very wide frequency range.

In order to improve PF for CRM flyback PFC converter, many control methods [16]–[19] have been studied. By using the input voltage and the voltage across the auxiliary winding of the flyback transformer to modulate the on-time of the main switch [17] or the peak envelope of primary current [18], sinusoidal input current and unity PF can be achieved. The research in [19] suggests a modified variable frequency one-cycle control for CRM flyback PFC converter, and unity PF can be also obtained. To further simplify the control circuit and the parameter design, Ref. [16] added a simple and low cost analog divider into traditional COT control circuit, which only requires operation amplifiers, signal switches, and RC filter. Although these aforementioned researches can obtain unity power factor and low THD, their variation range of switching frequency becomes larger than that of tradition COT control.

In order to reducing the variation range of switching frequency for PFC converter operating in CRM, a variable on-time control method was proposed in [20]. By injecting a certain amount of third harmonic in the peak current reference signal, an optimal scheme for reducing variation range of switching frequency is obtained. A fixed switching frequency control strategy was researched in [21]. The on-time of the main switch decreases as the increase of the transient rectified input voltage, so that the switching frequency can be fixed in each half-line period. Although these two aforementioned control methods can reduce or fix the switching frequency for PFC converter operating in CRM, they all suffer from low PF and serious distortion of input current.

Recently, adaptive control technique [22] has become a research hotspot to improve the performance and the stability of power converters. In this paper, in order to obtain both benefits of constant duty cycle controlled DCM flyback PFC converter and COT controlled CRM flyback PFC converter, an adaptive off-time (AOT) controlled DCM flyback PFC converter is proposed. The proposed controller adaptively adjusts the off-time of the main switch according to the output voltage and the amplitude of the input voltage, so that the magnetizing current of transformer can exactly operate in CRM when the rectified input voltage gets the peak. The proposed control strategy brings the following advantages:

1) Compared to constant duty cycle control, the RMS current of the main switch and the diode, as well as the conduction loss are effectively reduced, and the same high efficiency with COT control is achieved;
2) theoretically unity PF and sinusoidal input current over universal input voltage range of 90∼264VAC can be obtained;
3) the switching frequency of AOT control keeps fixed during each line cycle, so the variation range of switching frequency is significantly reduced compared to COT control, which brings potential convenience in the electromagnetic interference (EMI) filter design.

This paper is organized as follows: In Section 2, the features of COT controlled CRM flyback PFC converter and constant duty cycle controlled CRM flyback PFC converter are well analyzed. In Section 3, the principle of the proposed control scheme is presented. The comparison analysis of the aforementioned three control schemes are given in Section 4. In Section 5, an experimental prototype has been built and tested, and detailed results are provided.

II. FLYBACK PFC CONVERTER WITH TRANDITIONAL CONTROL METHODS

A. COT CONTROL

According to [17], the input current of COT controlled CRM flyback PFC converter can expressed as

$$i_{\text{in\_COT}}(t) = \frac{T_{\text{on\_COT}}^2 V_{\text{m}} \sin(\omega t)}{2L_{\text{m}} T_{\text{s\_COT}}(t)} \tag{1}$$

where V_{m} and ω are the amplitude and angular frequency of AC input voltage, respectively, L_{m} is the primary magnetic inductance of the transformer, $T_{\text{on\_COT}}$ is the on-time of main switch, and $T_{\text{s\_COT}}$ is the switching period of COT controlled CRM flyback PFC converter, which can be obtained as

$$T_{\text{s\_COT}}(t) = \left(1 + \frac{V_{\text{m}}}{NV_{\text{o}}} |\sin(\omega t)|\right) T_{\text{on\_COT}} \tag{2}$$

where N is the transformer turns ratio $N_{\text{p}}/N_{\text{s}}$, N_{p} and N_{s} are the number of turns of the primary winding and secondary winding, respectively.

From (1∼2), and with the AC input voltage $v_{\text{in}} = V_{\text{m}} \cdot \sin(\omega t)$, the average input power within half-line period can be derived as

$$\begin{aligned} P_{\text{in}} &= \frac{2}{T_{\text{line}}} \int_0^{T_{\text{line}}/2} v_{\text{in}}(t) i_{\text{in\_COT}}(t) dt \\ &= \frac{1}{\pi} \int_0^{\pi} \frac{V_{\text{m}}^2 T_{\text{on\_COT}} \sin^2(\omega t)}{2L_{\text{m}} \left(1 + \frac{V_{\text{m}} \sin(\omega t)}{NV_{\text{o}}}\right)} d\omega t \end{aligned} \tag{3}$$

where T_{line} is the line cycle. Then Eq. (3) can be further simplified as

$$P_{\text{in}} = \frac{K_1 V_{\text{m}}^2 T_{\text{on\_COT}}}{2\pi L_{\text{m}}} \tag{4}$$

where K_1 is a coefficient with

$$K_1 = \int_0^{\pi} \frac{\sin^2(\omega t)}{1 + (V_{\text{m}}/NV_{\text{o}}) |\sin(\omega t)|} d\omega t \tag{5}$$

Assuming that the efficiency of the converter is 100%, i.e., $P_o = P_{in}$, and based on (4), the on-time of the main switch T_{on_COT} can be obtained as

$$T_{on\_COT} = \frac{2\pi L_m P_o}{K_1 V_m^2} \tag{6}$$

By substituting (2), and (6) into (1), the input current of COT controlled CRM flyback PFC converter can be obtained as

$$i_{in\_COT}(t) = \frac{\pi P_o \sin(\omega t)}{K_1 V_m \left[1 + \left(V_m / NV_o\right)|\sin(\omega t)|\right]} \tag{7}$$

It can be known from (7) that, due to the variation of $[1+V_m|\sin(\omega t)|/(NV_o)]$, the input current of COT controlled CRM flyback PFC converter is non-sinusoidal, and the distortion increases with the increase of V_m/NV_o.

B. CONSTANT DUTYC CYCLE CONTROL

According to [15], the input current of constant duty cycle controlled DCM flyback PFC converter can obtained as

$$i_{in\_CDC}(t) = \frac{V_m \sin(\omega t) D_{CDC}^2}{2L_m f_{s\_CDC}} \tag{8}$$

where f_{s_CDC} is the switching frequency, and D_{CDC} is the duty cycle corresponding to the on-time of main switch. The average input power over half-line period can be obtained as

$$P_{in} = \frac{2}{T_{line}} \int_0^{T_{line}/2} v_{in}(t) i_{in\_CDC}(t) dt = \frac{V_m^2 D_{CDC}^2}{4L_m f_{s\_CDC}} \tag{9}$$

Assuming $P_{in} = P_o$, D_{CDC} can be derived as

$$D_{CDC} = \frac{2}{V_m}\sqrt{L_m f_{s\_CDC} P_o} \tag{10}$$

As the duty cycle is fixed, the input current is sinusoidal. However, the RMS current of DCM flyback PFC converter flowing through the main switch at the primary side and the freewheeling diode at the secondary side are high, resulting in high conduction loss and low efficiency. The RMS current of the main switch of constant duty cycle controlled DCM flyback PFC converter in each switch cycle can be derived as

$$\begin{aligned} i_{p\_RMS\_SW\_CDC}(t) &= \sqrt{\frac{1}{T_{s\_CDC}} \int_0^{D_{CDC} T_s} \left(\frac{V_m |\sin(\omega t)|}{L_m} u\right)^2 du} \\ &= \frac{V_m |\sin(\omega t)|}{L_m f_{s\_CDC}} \sqrt{\frac{D_{CDC}^3}{3}} \end{aligned} \tag{11}$$

According to (10) and (11), the RMS current of the main switch over a half-line period can be obtained as

$$\begin{aligned} I_{p\_RMS\_CDC} &= \sqrt{\frac{1}{\pi} \int_0^{\pi} \left[i_{p\_RMS\_SW\_CDC}(\omega t)\right]^2 d\omega t} \\ &= \frac{2}{\sqrt{3} V_m} \sqrt[4]{\frac{P_o^3}{L_m f_{s\_CDC}}} \end{aligned} \tag{12}$$

It can be known from (12) that, as the increase of the switching frequency, the RMS current decreases. Therefore, low conduction loss can be achieved by increasing the switching frequency. While, in order to achieve sinusoidal input current, the magnetizing current of the transformer should always operate in DCM, thus the following condition should be met:

$$D_{CDC} + D_1 \le 1 \tag{13}$$

where D_1 is the duty cycle corresponding to the on-time of the freewheeling diode at the secondary side. Based on volt-second balance, it has

$$D_1 = \frac{V_m |\sin(\omega t)|}{NV_o} D_{CDC} \tag{14}$$

By substituting (10) and (14) into (13), it yields

$$\frac{2}{V_m}\sqrt{L_m f_{s\_CDC} P_o}\left(1 + \frac{V_m |\sin(\omega t)|}{NV_o}\right) \le 1 \tag{15}$$

It can be known from (15) that the magnetizing current of the transformer is apt to be continuous at the peak of the rectified input voltage, thus the condition can be rewritten as

$$\frac{2}{V_m}\sqrt{L_m f_{s\_CDC} P_o}\left(1 + \frac{V_m}{NV_o}\right) \le 1 \tag{16}$$

From (16), the critical switching frequency f_{s_max} for flyback PFC converter operating in DCM is obtained as

$$f_{s\_CDC} \le f_{s\_max} = \frac{V_m^2}{4L_m P_o (1 + V_m / NV_o)^2} \tag{17}$$

From (10) and (17), the on-time T_{on} and the off-time T_{off} of the main switch of DCM flyback PFC converter when $f_{s\_CDC} = f_{s\_max}$ can be respectively derived as

$$T_{on} = \frac{4L_m P_o}{V_m^2}\left(1 + \frac{V_m}{NV_o}\right) \tag{18}$$

$$T_{off} = \frac{4L_m P_o}{V_m^2}\left(1 + \frac{V_m}{NV_o}\right)\frac{V_m}{NV_o} \tag{19}$$

By combining (18) and (19), it has

$$T_{off} = \frac{V_m}{NV_o} T_{on} \tag{20}$$

When T_{on} and T_{off} meet (20), DCM flyback PFC converter can operate at the maximal switching frequency f_{s_max}, and the lowest conduction loss can be achieved.

III. ADAPTIVE OFF-TIME CONTROLLED DCM FLYBACK PFC CONVERTER

In order to achieve both the lowest conduction loss and unity power factor, an adaptive off-time (AOT) control strategy for DCM flyback PFC converter, as shown in Fig.1, is proposed. It can be seen from Fig. 1(a), the proposed AOT controller is composed of a photo-coupler, a peak voltage detection circuits, an error amplifier (EA), saw-tooth carrier generators, comparators, a RS flip-flop and operation circuit.

In the AOT controller, the output voltage V_o is sensed by the photo-coupler and fed to the error amplifier. V_{con} is

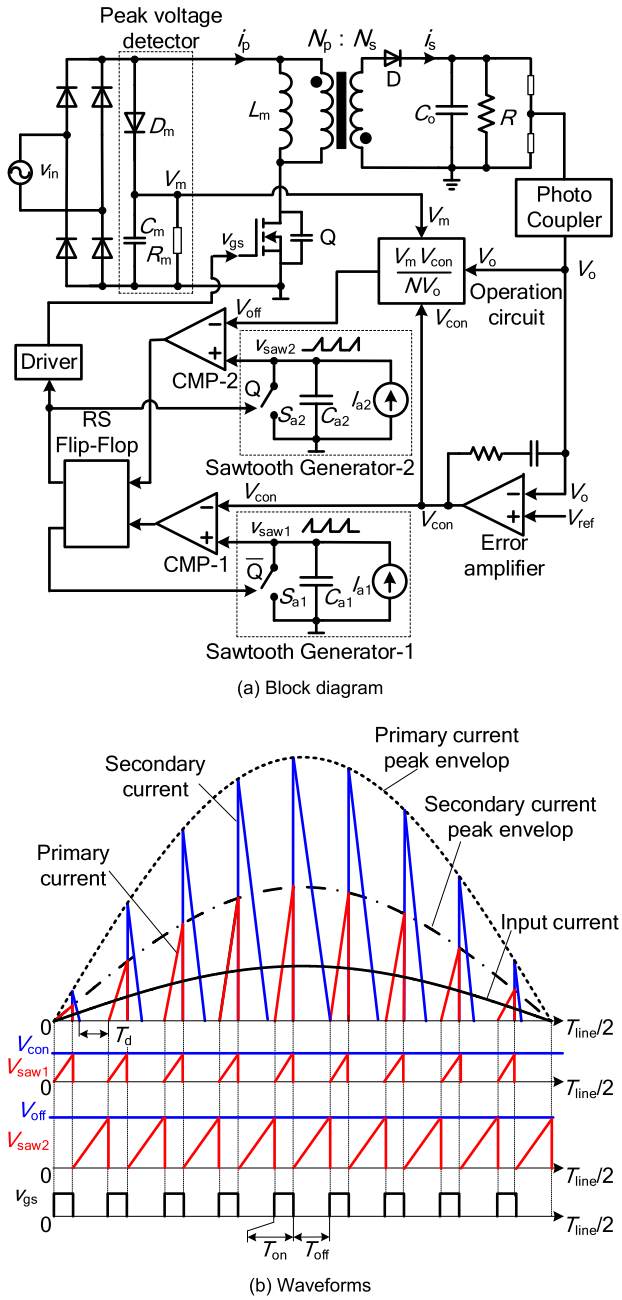

FIGURE 1. Block diagram and key waveforms of AOT controlled DCM flyback PFC converter.

the output of the error amplifier by compensating the error between the reference V_{ref} and output voltage V_o. V_m is the amplitude of AC input voltage v_{in}, which is obtained by a peak voltage detection circuit consisted of diode D_m, capacitor C_m and resistor R_m. In order to realize (20), V_o, V_m and V_{EA} are simultaneously fed to the operation circuit to generate the signal V_{off}, which is used to control the off-time of the main switch, with

$$V_{off} = \frac{V_{con} V_m}{NV_o} \tag{21}$$

Then, V_{con} and V_{off} are respectively sent to sawtooth generator-1 and sawtooth generator-2 to generate the control pulse v_{gs}.

Fig. 1(b) shows the operation principle. At the beginning of each switching cycle, the main switch Q is turned on, so the primary current i_p of the transformer increases from zero. Simultaneously, the auxiliary switch S_{a1} is turned off, thus the capacitor C_{a1} is charged by the current source I_{a1}, leading to the linear increase of v_{saw1}. When v_{saw1} increases to V_{con}, the output of comparator CMP-1 varies to high level, which resets v_{saw1} and makes the main switch Q and the auxiliary switch S_{a2} turn off, so the secondary current i_s of the transformer decreases, and v_{saw2} increases linearly. As v_{saw2} increases to V_{off}, the output of CMP-2 varies to high level, triggering the main switch Q to turn on again, and a new switch cycle begins.

It can be known from Fig. 1(b), the on-time T_{on_AOT} and the off-time T_{off_AOT} of the main switch Q can be respectively expressed as

$$T_{on\_AOT} = \frac{V_{con}}{k_1} \tag{22}$$

$$T_{off\_AOT} = \frac{V_{off}}{k_2} = \frac{V_m V_{con}}{NV_o k_2} \tag{23}$$

where $k_1 = I_{a1}/C_{a1}$ is the slop of v_{saw1}, $k_2 = I_{a2}/C_{a2}$ is the slop of v_{saw2}, and these two slopes are set as $k_1 = k_2$. By combining (22) and (23), it is evident that the relationship between T_{on_AOT} and T_{off_AOT} meets (20). Besides, it should be noted in Fig.1(b) that the time interval T_{zero}, when the transformer magnetizing current keeps zero, becomes shorter as the transient rectified input voltage increasing. When the rectified input voltage increases to the peak, T_{zero} is reduced to zero, and the transformer magnetizing current operates in CRM.

In steady state, the error signal V_{con}, the output voltage V_o, the amplitude of input voltage V_m, as well as the slopes k_1 and k_2 are constant, thus, T_{on_AOT}, T_{off_AOT} and the switching period

$$T_{s\_AOT} = T_{on\_AOT} + T_{off\_AOT} = \left(1 + \frac{V_m}{NV_o}\right) \cdot T_{on\_AOT} \tag{24}$$

also keep fixed in each half-line cycle.

According to Fig. 1(b), the input current of AOT controlled DCM flyback PFC converter can be obtained as

$$i_{in\_AOT}(t) = \frac{V_m T_{on\_AOT}^2}{2L_m T_{s\_AOT}} \sin(\omega t) \tag{25}$$

It can be known from (25) that the input current i_{in_AOT} of AOT controlled DCM flyback PFC converter is sinusoidal. According to (24) and (25), the average input power over a half-line period can be derived as

$$P_{in} = \frac{2}{T_{line}} \int_0^{T_{line}/2} v_{in}(t) i_{in\_AOT}(t) dt = \frac{V_m^2 T_{on\_AOT}}{4L_m(1 + V_m/NV_o)} \tag{26}$$

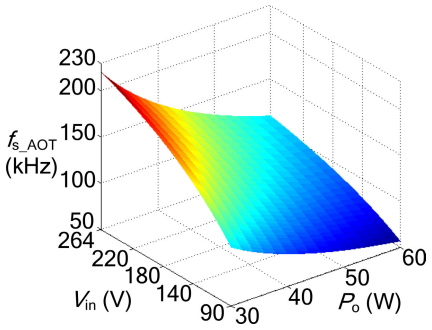

FIGURE 2. Surface of f_{s_AOT} as a function of V_{in} and P_o.

Assuming $P_o = P_{in}$, and based on (26), it is evident that T_{on_AOT} is equal to (18). As T_{on_AOT} and T_{on_off} also meets (20), it is easy to prove that the switching frequency f_{s_AOT} of AOT controlled DCM flyback PFC converter is exactly equal to f_{s_max} given in (17), therefore, the lowest RMS current and conduction loss can be both achieved.

Under the key circuit parameters: output voltage $V_o = 24$V, magnetizing inductance $L_m = 220\mu$H, turns ratio $N = 4$, output power range of $P_o = 30 \sim 60$W, and the RMS input voltage range of $V_{in} = V_m/\sqrt{2} = 90 \sim 264$VAC, the switching frequency f_{s_AOT} of AOT controlled DCM flyback PFC converter as a function of RMS input voltage V_{in} and output power P_o is plotted in Fig. 2. It can be seen from Fig. 2, f_{s_AOT} increases with the decrease of output power P_o and the increase of input voltage V_{in}, respectively The highest switching frequency is 220.6kHz when $P_o = 30$W and $V_{in} = 264$VAC, and the lowest switching frequency is 56.66kHz when $P_o = 60$W and $V_{in} = 90$VAC.

IV. COMPARISON ANALYSIS

A. SWITCHING FREQEUNCY

The switching cycle of COT controlled CRM flyback PFC converter can be obtained as [17]

$$T_{s\_COT}(t) = (1 + \frac{V_m|\sin(\omega t)|}{NV_o}) \cdot \frac{2\pi L_m P_o}{V_m^2 K_1} \qquad (27)$$

According to (17) and (27) and with the aforementioned key circuit parameters, Fig. 3 shows the switching frequency of AOT controlled DCM flyback PFC converter and COT controlled CRM flyback PFC converter over a half-line period.

It can be seen from Fig.3 that the switching frequency f_{s_COT} of COT controlled CRM flyback PFC converter varies within the half-line period, and the variation range is very large. Besides, f_{s_COT} is extremely high near the zero crossing of input voltage, which will result in great turn-off loss of the switch. While, the switching frequency f_{s_AOT} of AOT controlled DCM flyback PFC converter keeps fixed within the half-line period, and is slightly lower than the valley value of f_{s_COT}. Although f_{s_AOT} changes with the input voltage and of output power, the variation range is greatly reduced compared to that of COT control.

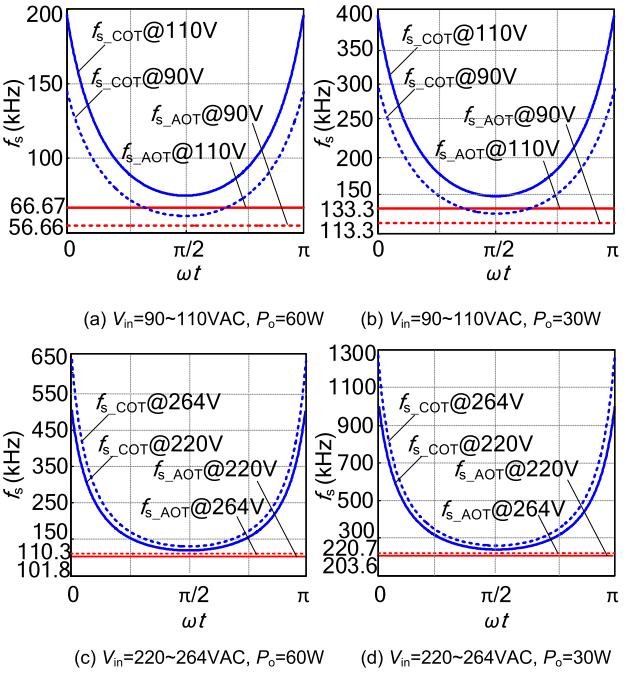

FIGURE 3. Switching frequency of AOT controlled and COT controlled flyback PFC converter.

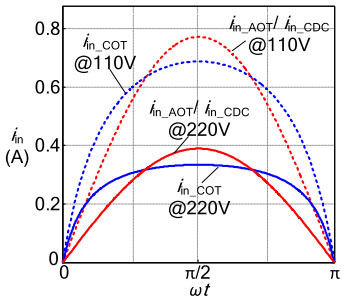

FIGURE 4. Input current of COT controlled, constant duty cycle controlled and AOT controlled flyback PFC converter.

B. PF AND INPUT CURRENT THD

Based on the aforementioned key parameters, and according to (7), (8) and (25), the input current of COT controlled CRM flyback PFC converter, constant duty cycle controlled and AOT controlled DCM flyback PFC converter when $P_o = 60$W within a half line cycle is plotted in Fig.4. It can be seen from Fig. 4, the input current of AOT controlled and constant duty cycle controlled DCM flyback PFC converter are sinusoidal, while the input current of COT controlled CRM flyback PFC converter is distorted, and the distortion when $V_{in} = 220$VAC is evidently larger than that when $V_{in} = 110$VAC.

According to [17], when the AC input voltage is sinusoidal, the PF and input current THD are expressed as

$$\mathrm{PF} = \frac{\frac{2}{T_{line}}\int_0^{T_{line}/2} v_{in}(t) i_{in}(t) dt}{\frac{V_m}{\sqrt{2}} \cdot \sqrt{\frac{2}{T_{line}}\int_0^{T_{line}/2} i_{in}^2(t) dt}} \qquad (28)$$

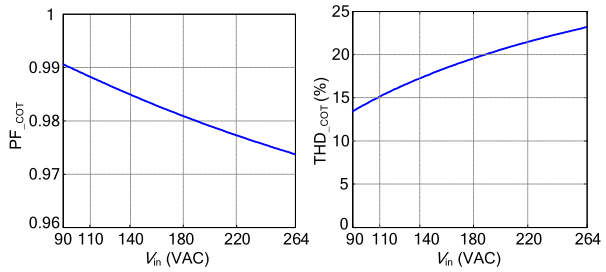

(a) $PF_{\_COT}$ (b) $THD_{\_COT}$

FIGURE 5. PF and input current THD of COT controlled CRM flyback PFC converter for different V_{in}.

$$\mathrm{THD} = \sqrt{\frac{1}{\mathrm{PF}^2} - 1} \tag{29}$$

By substituting (8), (25) into (28) and (29), it can be found that the PF and the input current THD of constant duty cycle controlled and AOT controlled DCM flyback PFC converter are unity and zero, respectively.

By substituting (7) into (28), the PF of COT controlled CRM flyback PFC converter is obtained as

$$\mathrm{PF\_COT} = \frac{\frac{\sqrt{2}}{\pi}\int_0^{\pi} \frac{\sin^2(\omega t)}{1+(V_m/NV_o)|\sin(\omega t)|} d\omega t}{\sqrt{\frac{1}{\pi}\int_0^{\pi}\left[\frac{\sin(\omega t)}{1+(V_m/NV_o)|\sin(\omega t)|}\right]^2 d\omega t}} \tag{30}$$

Based on the aforementioned key parameters, and according to (29) and (30), Fig.5 shows the PF and input current THD of COT controlled CRM flyback PFC converter for different RMS input voltage.

As is shown, $PF_{\_COT}$ decreases with the increases of RMS input voltage, and the minimum of PF_COT is 0.9742. $THD_{\_COT}$ increases with the increases of RMS input voltage, and the maximum of $THD_{\_COT}$ is 23.16%.

C. RMS CURRENT AND PEAK CURRENT

The RMS current of the main switch Q at the primary side for COT control in each switching cycle can be derived as

$$\begin{aligned} i_{\mathrm{p\_RMS\_sw\_COT}}(t) &= \sqrt{\frac{1}{T_{\mathrm{s\_COT}}}\int_0^{T_{\mathrm{on\_COT}}}\left(\frac{V_m|\sin(\omega t)|}{L_m}u\right)^2 du} \\ &= \frac{T_{\mathrm{on\_COT}}V_m}{\sqrt{3}L_m}\sqrt{\frac{\sin^2(\omega t)}{1+V_m|\sin(\omega t)|/NV_o}} \end{aligned} \tag{31}$$

From (6) and (31), the RMS current of the main switch over half-line period can be derived as

$$\begin{aligned} I_{\mathrm{p\_RMS\_COT}} &= \sqrt{\frac{1}{\pi}\int_0^{\pi}\left[i_{\mathrm{p\_RMS\_sw\_COT}}(\omega t)\right]^2 d\omega t} \\ &= \frac{2P_o}{V_m}\sqrt{\frac{\pi}{3K_1}} \end{aligned} \tag{32}$$

The RMS current of the diode D at the secondary side for COT control in each switching cycle is derived as

$$\begin{aligned} i_{\mathrm{s\_RMS\_sw\_COT}}(t) &= \sqrt{\frac{1}{T_{\mathrm{s\_COT}}}\int_0^{T_d}\left(\frac{V_o}{(L_m/N^2)}u\right)^2 du} \\ &= \frac{NT_{\mathrm{on\_COT}}}{L_m}\sqrt{\frac{V_m^3|\sin^3(\omega t)|}{3(NV_o+V_m\sin(\omega t))}} \end{aligned} \tag{33}$$

where $T_d = V_m|\sin(\omega t)| \cdot T_{\mathrm{on\_COT}}/(NV_o)$ is the on-time of the diode D. From (6) and (33), the RMS current of the diode D over half-line period can be derived as

$$\begin{aligned} I_{\mathrm{s\_RMS\_COT}} &= \sqrt{\frac{1}{\pi}\int_0^{\pi}\left[i_{\mathrm{s\_RMS\_sw\_COT}}(\omega t)\right]^2 d\omega t} \\ &= \frac{2N\sqrt{\pi}P_o}{K_1V_m^2}\sqrt{\int_0^{\pi}\frac{V_m^3|\sin^3(\omega t)|}{3(NV_o+V_m\sin(\omega t))}d\omega t} \end{aligned} \tag{34}$$

Similarly, the RMS current of the main switch Q and diode D for AOT control over half-line period can be respectively derived as

$$I_{\mathrm{p\_RMS\_AOT}} = \frac{4P_o}{V_m}\sqrt{\frac{1+V_m/(NV_o)}{6}} \tag{35}$$

$$I_{\mathrm{s\_RMS\_AOT}} = \frac{8NP_o(1+V_m/NV_o)}{V_m^2}\sqrt{\frac{V_m^3}{9\pi(V_m+NV_o)}} \tag{36}$$

The RMS current of the diode D for constant duty cycle control over half-line period can be derived as

$$i_{\mathrm{s\_RMS\_CDC}}(t) == \frac{V_oN^2}{L_m}\sqrt{\frac{32\left(L_mf_{\mathrm{s\_CDC}}P_o\right)^{\frac{3}{2}}}{9\pi N^3V_o^3\cdot f_{\mathrm{s\_CDC}}^2}} \tag{37}$$

The peak current of the switch Q for AOT control, COT control and constant duty cycle control over half-line period can be respectively derived as

$$I_{\mathrm{p\_peak\_AOT}} = \frac{V_mT_{\mathrm{on\_AOT}}}{L_m} = \frac{4P_o}{V_m}\left(1+\frac{V_m}{NV_o}\right) \tag{38}$$

$$I_{\mathrm{p\_peak\_COT}} = \frac{V_mT_{\mathrm{on\_COT}}}{L_m} = \frac{2\pi P_o}{K_1V_m} \tag{39}$$

$$I_{\mathrm{p\_peak\_CDC}} = \frac{V_mD_{\mathrm{CDC}}}{L_mf_{\mathrm{s\_CDC}}} = 2\sqrt{\frac{P_o}{L_mf_{\mathrm{s\_CDC}}}} \tag{40}$$

Besides, the relationship between the peak current of the diode D and the switch Q for flyback converter is $i_{\mathrm{s\_peak}} = N \cdot i_{\mathrm{p\_peak}}$. According to (12), (32), (34∼40), and under the aforementioned key parameters, the RMS current and the peak current of the switch Q and the diode D of flyback PFC converter with these aforementioned three control methods for different RMS input voltage when $P_o = 60$W are plotted in Fig. 6 and Fig. 7, respectively.

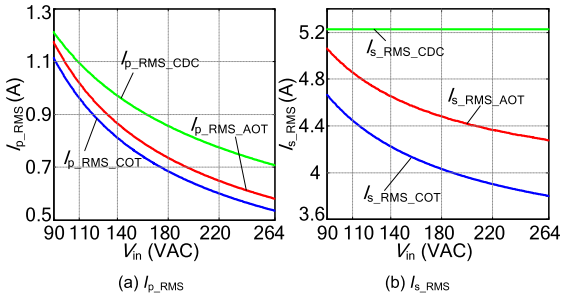

FIGURE 6. The RMS current of the main switch and the diode of flyback PFC converter with the aforementioned three control methods for different V_{in}.

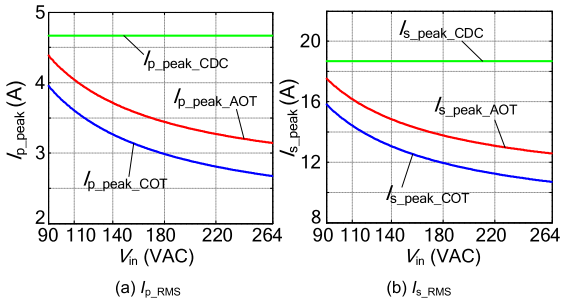

FIGURE 7. The peak current of the main switch and the diode of flyback PFC converter with the aforementioned three control methods for different V_{in}.

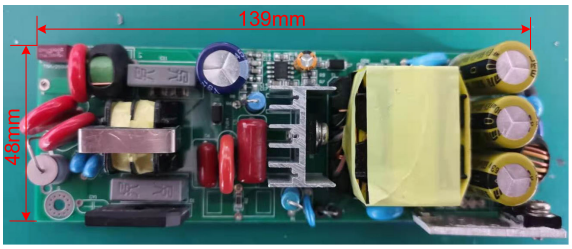

FIGURE 8. Experimental prototype.

The switching frequency f_{s_CDC} of constant duty cycle controlled DCM flyback PFC converter is set as 50kHz. It can be seen from Fig. 6 and Fig. 7 that the RMS current and the peak current of the switch Q and the diode D of AOT control and COT control are evidently lower than that of constant duty cycle control, particularly at high RMS input voltage. Besides, it should be noted that COT control features slightly lower RMS current and peak current than those of AOT control, as the magnetizing current of COT control always operates in CRM within half-line period, while the magnetizing current of AOT control only operates in CRM when the transient rectified input voltage gets to the peak.

V. EXPERIMENTAL VERIFICATION

In order to verify the validity of the proposed AOT control, a 60W prototype has been built and tested in the laboratory, as shown in Fig. 8. In the experimental platform, the input AC power supply is Itech IT7625, and the electronic load Itech IT8617 is utilized as the output of the prototype. The

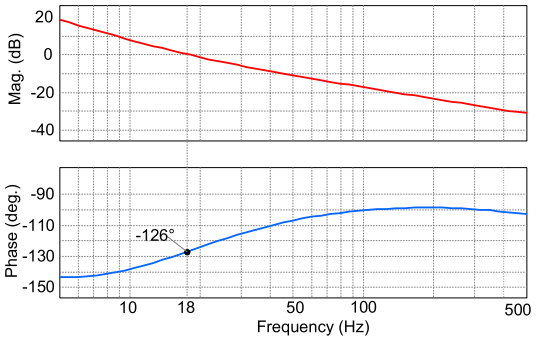

FIGURE 9. Bode plot of AOT control loop.

experimental waveforms are measured by the oscilloscope Tektronix TDS3034B.

The specifications of the prototype are as follows:

1) RMS input voltage: $V_{in} = 90 \sim 264$VAC;
2) line frequency: $f_{line} = 50$Hz;
3) output voltage: $V_o = 24$V;
4) output power: $P_o = 30 \sim 60$W;

The main components of the power circuit are list as follows:

1) transformer: $L_m = 220\mu$H, $N = 4$;
2) output capacitance: $C = 3000\mu$F.
3) Primary switch: SMK1265
4) Secondary diode: MUR1020CT
5) Input rectifier bridge: GBU1504

In the AOT controller shown in Fig. 1(a), a proportional-integral (PI) compensator is utilized as the error amplifier, and the transfer function of PI compensator is given as

$$H_V(s) = K_P + \frac{K_I}{s} \tag{41}$$

where K_P and K_I are the proportion and integration coefficients of $H_V(s)$, respectively. According to the control loop design procedures of PFC converter [23], K_P and K_I, as well as the output voltage sensing gain are designed as 0.35 35 and 0.1, respectively. Since the PFC converter is a time-varying system, in order to analyze the bandwidth and stability of the control loop, the "frozen coefficients" method [5] is utilized. The system is frozen at the point that is assumed to be the most critical for its stability, i.e., when input voltage $v_{rec} = V_m|\sin(\omega t)|$ gets the peak and load is full. Then, based on the aforementioned specifications and parameters, the simulation of AOT controlled DCM flyback PFC converter in the frequency domain is performed when $V_{in} = 264$V and $P_o = 60$W, and the corresponding Bode plots of the control loop is shown in Fig. 9. It can be seen from Fig. 9 that, the bandwidth of the control loop is 18Hz, which is within the limit of 20Hz for PFC system [5]. The phase margin is 54°, which is sufficiently larger than the general stability requirement of 45°.

Fig. 10 and Fig. 11 show the AC input voltage v_{in}, input current i_{in} and output voltage V_o of AOT controlled and COT controlled flyback PFC converter, when V_{in} is 90VAC, 110VAC, 220VAC and 264VAC, respectively. It can be known

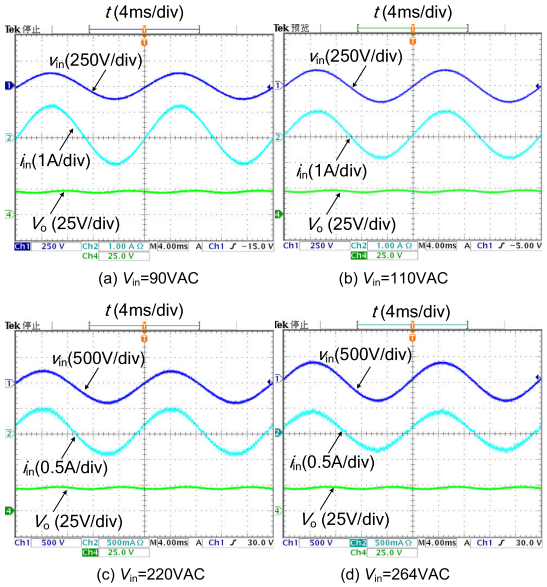

FIGURE 10. Experimental waveforms of AOT controlled DCM flyback PFC converter.

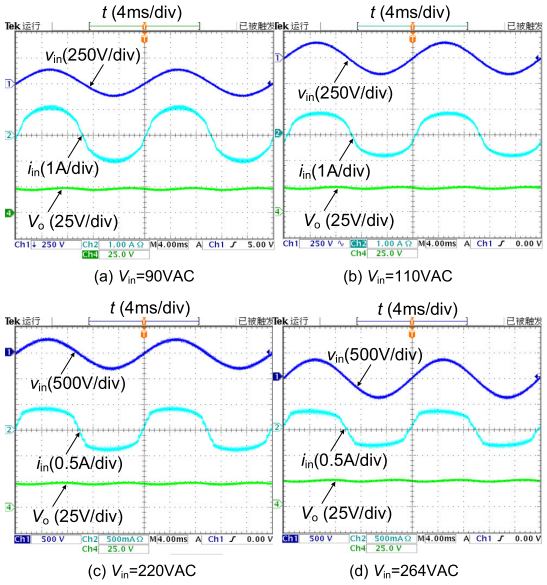

FIGURE 11. Experimental waveforms of COT controlled CRM flyback PFC converter.

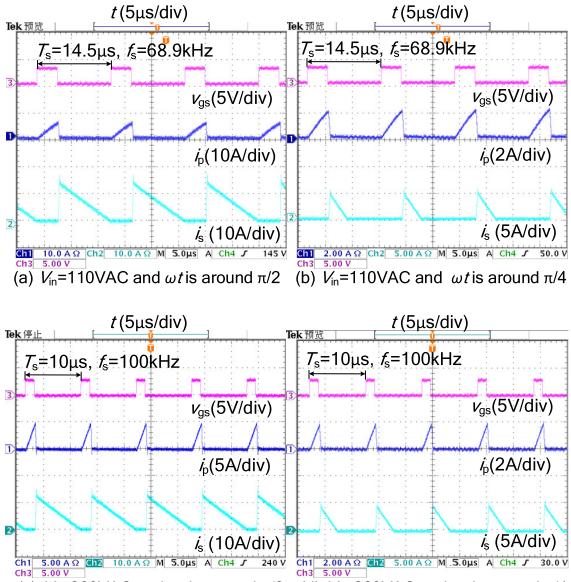

FIGURE 12. Zoomed-in waveforms of AOT controlled DCM flyback PFC converter.

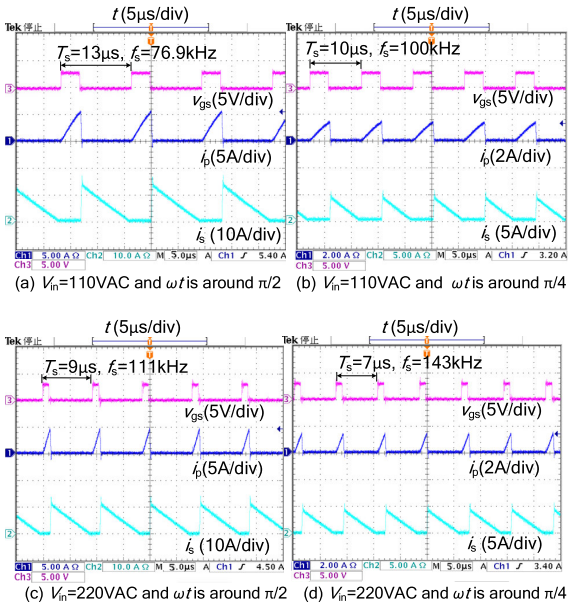

FIGURE 13. Zoomed-in waveforms of COT controlled CRM flyback PFC converter.

from Fig. 10 and Fig. 11 that the input current of AOT controlled DCM flyback PFC converter always maintains sinusoidal over the universal input voltage range. While, the input current of COT controlled CRM flyback PFC converter is distorted obviously, and the distortion increases with the increase of input voltage.

Fig. 12 and Fig. 13 show the zoomed-in waveforms of drive signal v_{gs}, primary current i_p and secondary current i_s of AOT controlled DCM flyback PFC converter and COT controlled CRM flyback PFC converter under RMS input voltage of 110VAC, 220VAC and output power of 60W.

It can be seen from Fig. 12 that when $V_{in} = 110$VAC, the switching period is always maintained at 14.5μs when the phase of AC input voltage ωt is around $\pi/2$ and $\pi/4$; When $V_{in} = 220$VAC, the switching period is always maintained at 10μs when ωt is around $\pi/2$ and $\pi/4$. Thus, the switching frequency of AOT controlled DCM flyback PFC converter can keep fixed in steady state. Besides, it should be noted in Fig.12(a) and (c) that the magnetizing current of the transformer operates in CRM when $\omega t = \pi/2$. While, in Fig. 13, the switching frequency of COT controlled CRM flyback PFC converter changes with the change of ωt, and the variation range of switch frequency is obviously larger than that of AOT controlled DCM flyback PFC converter.

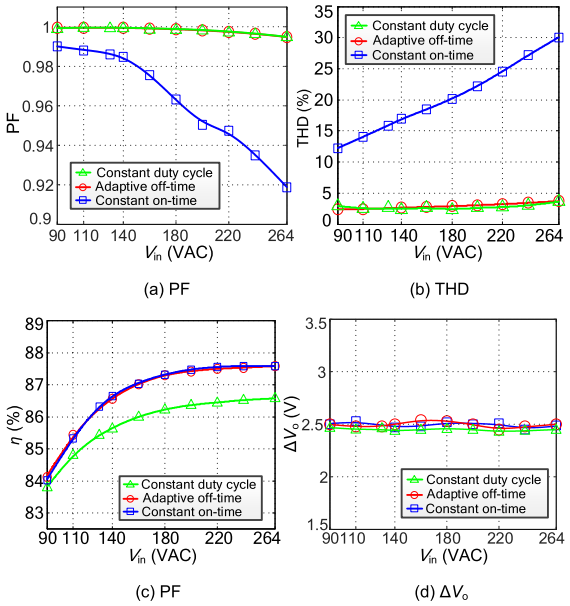

FIGURE 14. Experimental results of AOT controlled, COT controlled and constant duty cycle controlled flyback PFC converter for different V_{in}.

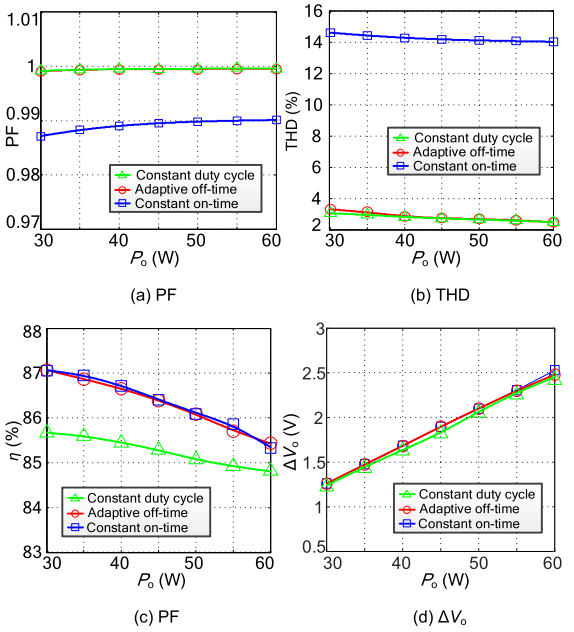

FIGURE 15. Experimental results of AOT controlled, COT controlled and constant duty cycle controlled flyback PFC converter for different P_o.

Fig. 14 shows the measured PF, THD, efficiency η and output voltage ripple ΔV_o of COT controlled CRM flyback PFC converter, AOT controlled and constant duty cycle controlled DCM flyback PFC converter for the variation of RMS input voltage when output power is 60W. As is shown in Fig. 14(a) that the PF of AOT control and constant duty cycle control is always higher than 0.994 over the RMS input voltage range of 90∼264VAC, while the PF of COT control decreases with the increase of V_{in}, and the minimal PF is 0.92. It can be seen from Fig. 14(b) that the input current THD of AOT control and constant duty cycle control is lower than 4%, while the maximal THD of COT control is 30%. It can be seen from Fig. 14(c) that the efficiency of AOT control is very close to that of COT control, and the efficiency of these two controls are significantly higher that of constant duty cycle control, especially at high input voltage. As is shown in Fig. 14(d), these three control methods share the same output voltage ripple of 2.5V over the universal input voltage range.

Fig. 15 shows the measured PF, THD, efficiency η and output voltage ripple ΔV_o of flyback PFC converter with the aforementioned three control methods for different output power when RMS input voltage is 110VAC. It can be seen from Fig. 15(a) and (b) that the PF and input current THD of AOT control and constant duty cycle control are very close. Besides, the PF and THD of AOT control and constant duty cycle control are evidently better than those of COT control. It can be Fig. 15(c) that the efficiency of AOT control and COT control are very close, which are significantly higher than that of constant duty cycle control. As is shown in Fig. 15(d), the output voltage ripple of these three control methods are very close, and increase with the increase of output power.

Table 1 gives the comparison of state-of-the-art for these three control methods. It can be easily found in Tab. 1 that the proposed AOT control has the advantages of both constant duty cycle control and COT control, i.e., high PF, low input current THD and high efficiency. Besides, these three control methods share the same output voltage ripple.

TABLE 1. Comparison of state-of-the-art.

	AOT	Constant duty cycle	COT
PF	Theoretical unit	Theoretical unit	Lower than 0.99
Input current THD	Theoretical zero	Theoretical zero	Higher than 12.5%
Peak efficiency	87.6%	86.5%	87.6%
Maximal output voltage ripple	2.51V	2.51V	2.5V
Current stress of MOSFET and diode	Low	High	Low
Variation range of f_s	Small	None	Large

VI. CONCLUSION

This paper proposes an adaptive off-time controlled DCM flyback PFC converter. According to the output voltage and the amplitude of line voltage, the proposed controller adaptively adjusts the off-time of the main switch, so that the magnetizing current of the transformer can exactly operate in CRM. This operation mode can effectively reduce the conduction loss of the main switch and increase efficiency, and on the other hand, similar with constant duty cycle control, the duty cycle and the switch period of AOT control remains fixed during each line cycle, therefore, theoretical

unity PF and sinusoidal input current can be also obtained over universal input voltage range. Moreover, the variation range of the switching frequency of AOT control strategy is greatly narrowed compared to that of COT control, which will bring potential convenience in the input filter design. A 60W experimental prototype has been built to verify the theoretical analysis. Experimental results show the minimal PF of AOT control and constant duty cycle control is 0.994, which is significantly higher the minimal PF 0.92 of COT control, and the highest efficiency of AOT control and COT control is 87.6%, which is obviously higher than the highest efficiency 86.5% of constant duty cycle control.

REFERENCES

[1] M. M. Jovanovic and Y. Jang, "State-of-the-art, single-phase, active power-factor-correction techniques for high-power applications—An overview," *IEEE Trans. Ind. Electron.*, vol. 52, no. 3, pp. 701–708, Jun. 2005.
[2] O. Garcia, J. A. Cobos, R. Prieto, P. Alou, and J. Uceda, "Single phase power factor correction: A survey," *IEEE Trans. Power Electron.*, vol. 18, no. 3, pp. 749–755, May 2003.
[3] C. Qiao, G. Feng, and K. M. Smedley, "A topology survey of single-stage power factor corrector with a boost type input-current-shaper," *IEEE Trans. Power Electron.*, vol. 16, no. 3, pp. 360–368, May 2001.
[4] Z. Chen, P. Davari, and H. Wang, "Single-phase bridgeless PFC topology derivation and performance benchmarking," *IEEE Trans. Power Electron.*, vol. 35, no. 9, pp. 9238–9250, Sep. 2020, doi: 10.1109/tpel.2020.2970005.
[5] H. Luo, J. Xu, D. He, and J. Sha, "Pulse train control strategy for CCM boost PFC converter with improved dynamic response and unity power factor," *IEEE Trans. Ind. Electron.*, vol. 67, no. 12, pp. 10377–10387, Dec. 2020.
[6] Y.-S. Kim, W.-Y. Sung, and B.-K. Lee, "Comparative performance analysis of high density and efficiency PFC topologies," *IEEE Trans. Power Electron.*, vol. 29, no. 6, pp. 2666–2679, Jun. 2014.
[7] H.-J. Chiu, Y.-K. Lo, H.-C. Lee, S.-J. Cheng, Y.-C. Yan, C.-Y. Lin, T.-H. Wang, and S.-C. Mou, "A single-stage soft-switching flyback converter for power-factor-correction applications," *IEEE Trans. Ind. Electron.*, vol. 57, no. 6, pp. 2187–2190, Jun. 2010.
[8] J.-J. Lee, J.-M. Kwon, E.-H. Kim, W.-Y. Choi, and B.-H. Kwon, "Single-stage single-switch PFC flyback converter using a synchronous rectifier," *IEEE Trans. Ind. Electron.*, vol. 55, no. 3, pp. 1352–1365, Mar. 2008.
[9] D. G. Lamar, M. Arias, A. Rodriguez, A. Fernandez, M. M. Hernando, and J. Sebastian, "Design-oriented analysis and performance evaluation of a low-cost high-brightness LED driver based on flyback power factor corrector," *IEEE Trans. Ind. Electron.*, vol. 60, no. 7, pp. 2614–2626, Jul. 2013.
[10] H.-L. Cheng, Y.-N. Chang, C.-H. Chang, S.-Y. Hsieh, and C.-A. Cheng, "A novel high-power-factor AC/DC LED driver with dual flyback converters," *IEEE J. Emerg. Sel. Topics Power Electron.*, vol. 7, no. 1, pp. 555–564, Mar. 2019.
[11] S. P. Yang, J. L. Lin, and S. J. Chen, "Dynamics analysis of a low-voltage stress single-stage high-power factor correction AC/DC flyback converter," *IET Power Electron.*, vol. 5, no. 9, pp. 1624–1633, Nov. 2012.
[12] Y.-C. Chang and C.-M. Liaw, "Design and control for a charge-regulated flyback switch-mode rectifier," *IEEE Trans. Power Electron.*, vol. 24, no. 1, pp. 59–74, Jan. 2009.
[13] X. Xie, J. Wang, C. Zhao, Q. Lu, and S. Liu, "A novel output current estimation and regulation circuit for primary side controlled high power factor single-stage flyback LED driver," *IEEE Trans. Power Electron.*, vol. 27, no. 11, pp. 4602–4612, Nov. 2012.
[14] J.-W. Shin, S.-J. Choi, and B.-H. Cho, "High-efficiency bridgeless flyback rectifier with bidirectional switch and dual output windings," *IEEE Trans. Power Electron.*, vol. 29, no. 9, pp. 4752–4762, Sep. 2014.
[15] K. Yao, X. Fu, and J. Lv, "DCM flyback PFC converter with optimum utilization control of switching cycles," in *Proc. IEEE Energy Convers. Congr. Expo. (ECCE)*, Sep. 2015, pp. 2445–2452.
[16] C. Zhao, J. Zhang, and X. Wu, "An improved variable on-time control strategy for a CRM flyback PFC converter," *IEEE Trans. Power. Electron.*, vol. 32, no. 2, pp. 915–920, Feb. 2017.
[17] T. Yan, J. Xu, F. Zhang, J. Sha, and Z. Dong, "Variable-on-time-controlled critical-conduction-mode flyback PFC converter," *IEEE Trans. Ind. Electron.*, vol. 61, no. 11, pp. 6091–6099, Nov. 2014.
[18] J. He, J. Xu, and T. Yan, "Peak current-controlled CRM flyback PFC converter with square of line voltage-compensated primary current envelope," *Electron. Lett.*, vol. 51, no. 9, pp. 684–686, Apr. 2015.
[19] H. Dong, X. Xie, K. Peng, J. Li, and C. Zhao, "A variable-frequency one-cycle control for BCM flyback converter to achieve unit power factor," in *Proc. IECON-40th Annu. Conf. IEEE Ind. Electron. Soc.*, Oct. 2014, pp. 1161–1166.
[20] X. Wang, K. Yao, and J. Zhang, "Reducing the switching frequency variation range for CRM buck PFC converter by variable on-time control," in *Proc. IEEE Appl. Power Electron. Conf. Expo. (APEC)*, Mar. 2016, pp. 572–579.
[21] K. Yao, Y. Wang, J. Guo, and K. Chen, "Critical conduction mode boost PFC converter with fixed switching frequency control," *IEEE Trans. Power Electron.*, vol. 33, no. 8, pp. 6845–6857, Aug. 2018.
[22] L. Liu, W. X. Zheng, and S. Ding, "An adaptive SOSM controller design by using a sliding-mode-based filter and its application to buck converter," *IEEE Trans. Circuits Syst. I, Reg. Papers*, vol. 67, no. 7, pp. 2409–2418, Jul. 2020.
[23] R. Ghosh and G. Narayanan, "A simple method to improve the dynamic response of single-phase PWM rectifiers," *IEEE Trans. Ind. Electron.*, vol. 55, no. 10, pp. 3627–3634, Oct. 2008.

HUAN LUO (Member, IEEE) was born in Sichuan, China, in 1990. He received the B.S. degree in electrical engineering from Southwest Jiaotong University, Chengdu, China, in 2012, the M.S. degree in power system from Sichuan University, Chengdu, in 2015, and the Ph.D. degree in electrical engineering from Southwest Jiaotong University, in 2020.

He is currently a Lecturer with Sichuan University. His research interests include the control technique of switching-mode power supplies, single-phase power factor correction, and renewable power systems.

TIANLEI ZANG (Member, IEEE) received the Ph.D. degree from Southwest Jiaotong University, in 2017. From 2017 to 2020, he holds a postdoctoral position with Tsinghua University. He is currently an Associate Research Fellow with the College of Electrical Engineering, Sichuan University. His research interests include energy internet, fault analysis, and safety assessment of energy electrical systems.

SHI CHEN (Member, IEEE) received the B.S. and Ph.D. degrees in power system from Sichuan University, Chengdu, China, in 2000 and 2014, respectively.

Since 2003, he has been with the School of Electrical Engineering, Sichuan University, where he has been an Associate Professor of power system, since 2017. His research interests include stability, operation, optimization of power systems, and power grid planning.

BUXIANG ZHOU (Member, IEEE) received the B.S. and M.S. degrees in power system from Sichuan University, Chengdu, China, in 1986 and 1993, respectively, and the Ph.D. degree in power system from Chongqing University, in 1998.

Since 1994, he has been with the School of Electrical Engineering, Sichuan University, where he has been a Professor of power system, since 1998. His research interests include dispatch, operation, control of power systems, and information technique of power systems.